Advancing neodymium single-band nanothermometry

Artiom Skripka, Alexandre Morinvil, Marija Matulionyte, Ting Cheng and Fiorenzo Vetrone*

Centre Énergie, Matériaux et Télécommunications, Institut National de la Recherche Scientifique, Université du Québec, 1650 Boul. Lionel-Boulet, Varennes, QC, J3X 1S2, Canada

Corresponding author: *vetrone@emt.inrs.ca

Table of Contents

Experimental

Materials

Lu_2O_3 (REacton, 99.9%), Nd_2O_3 (REacton, 99.999%), Y_2O_3 (REacton, 99.999%), trifluoroacetic acid (99%), 1-octadecene (ODE, 90%), and oleic acid (OA, 90%) were purchased from Alfa Aesar (USA). Lithium trifluoroacetate (97%) and oleylamine (OM, 70%) were obtained from Sigma-Aldrich (USA). All chemicals were used without further purification.

Precursor preparation

Rare earth (RE) trifluoroacetate precursors (1 mmol) for the synthesis of $LiLuF_4:Nd^{3+}$ core RENPs of different Nd^{3+} doping (1, 2.5 and 5 %) were prepared by mixing stoichiometric quantities of Lu_2O_3 and Nd_2O_3 (total amount of oxides corresponding to 0.5 mmol) in each case with 5 mL trifluoroacetic acid and 5 mL of water in 100 mL three-neck round bottom flasks. The mixtures were refluxed under vigorous stirring at 80 ºC until the solutions became clear, at which point the temperature was decreased to 60 ºC for residual trifluoroacetic acid and water to evaporate. Precursors for $LiLuF_4$, $LiYF_4$, or $LiGdF_4$ shells were prepared in analogous fashion, out of 1 mmol of Lu_2O_3, Y_2O_3, or Gd_2O_3 respectively.

RENP synthesis

RENPs were prepared via modified two-step thermal decomposition method, synthesizing first nuclei (FN), which serve as seeds to form the desired core RENPs.[1]

FN formation: Dried RE trifluoroacetate precursors were mixed with 1.0 mmol of lithium trifluoroacetate, 5 mL each of OA and OM and 10 mL of ODE. Solution was degassed at 110 ºC under vacuum and magnetic stirring for 30 min. After degassing, the solution was back-filled with Ar, the temperature was raised to 330 ºC, and left to react for 1 h. Maintaining the Ar flow and stirring, the solution was then cooled to room temperature (RT).

Core synthesis: Core RENPs were formed by the stabilization of FN with excess of OA. FN (0.5 mmol, ~ 10 mL of stock solution) were mixed with 15 mL each of OA and ODE in a 100 ml three-neck round bottom flask. The solution was degassed at 110 ºC under vacuum and magnetic stirring for 30 min. Then, back-filled with Ar and the temperature was raised to 330 ºC, at which point reaction continued for 1 h. After cooling to RT, a small portion (0.5 mL) of core RENPs was sampled for characterization.

Core shelling: Core/shell RENPs were prepared by epitaxial growth of the shell on the preformed cores *via* the hot-injection approach. Approximately 0.1 mmol of core RENPs were mixed in 100 mL three-neck round bottom flask together with equal parts of OA and ODE up to a total volume of 20 mL (Solution A). Seperately, Solution B was prepared by mixing approximately 0.25 mmol of desired RE shelling precursors together with 0.25 mmol of lithium trifluoroacetate, and 10 mL each of OA and ODE. Both solutions were degassed under vacuum and magnetic stirring at 110 ºC for 30 min. After degassing, Solution A was back-filled with Ar and the temperature was raised to 315 ºC. Solution B was then injected into the reaction vessel containing Solution A using a syringe and pump system (Harvard Apparatus Pump 11 Elite, USA) at a 1.5 mL/min injection rate. The mixture was left at a temperature of 315 ºC under vigorous stirring for 60 min, at which point it was cooled to RT. Resultant core/shell RENPs were precipitated with ethanol, and washed sequentially with hexane/ethanol, toluene/acetone and hexane/ethanol (1/4 v/v in each case) *via* centrifugation (5400 RCF). Finally, RENPs were re-dispersed in hexane for further structural characterization and transfer to water.

RENP transfer to water

RENPs were transferred to water following ligand removal procedure.[2] Briefly, 10 mg of oleate-capped RENPs were mixed with 5 mL each of hexane and distilled water (pH ~ 3-4; adjusted with HCl) and left under vigorous stirring for 24 h at RT. Aqueous and organic phases were separated with the separatory funnel, and RENPs contained in the aqueous phase were precipitated with acetone *via* centrifugation (12000 RCF). The obtained pellet was re-dispersed in 5 mL of distilled water (pH ~ 3-4) and left stirring for an additional 3 h at RT. RENPs were then precipitated and washed twice with a mixture of water/acetone (1/4 v/v) *via* centrifugation. Finally, ligand-free RENPs were re-dispersed in distilled water, and used without further purification for optical and thermometric studies.

Structural characterization

The crystallinity and phase of the core and core/shell RENPs were determined *via* X-ray powder diffraction (XRD) analysis with a Bruker D8 Advance Diffractometer (USA) using CuKα radiation. The morphology and size distribution of the core and core/shell RENPs were investigated by transmission electron microscopy (TEM, Philips Tecnai 12, USA). The particle size was determined from TEM images using ImageJ image analysis software with set size of 500 to 1000 individual particles per sample.

Optical characterization

Near-infrared (NIR) photoluminescence (PL) of different RENPs was recorded under 793 nm laser diode excitation (CNI, China; 684 mW ≃ 49 W/cm^2) with a Shamrock 500i monochromator (Andor, Ireland) equipped with an iDus InGaAs 1.7 NIR detector (Andor, Ireland). In order to remove any stray light from the excitation source long pass (LP) 830 nm filter (Semrock, Inc., USA) was used.

Thermosensitivity characterization

The thermal response of RENPs was measured in the 20 to 45 ºC temperature (*T*) range at 5 ºC increments. The temperature was changed using a temperature controlled cuvette holder (qpod 2e by Quantum Northwest, Washington, USA). 10 min intervals were maintained between the measurements in order to reach thermal equilibrium at a set temperature. Nanothermometer characterizing parameters were calculated following the guidelines set by C. D. S. Brites et al.[3] PL intensity ratio (thermometric parameter - Δ) was estimated taking the ratio between the integrated intensities I_n and I_m (*n* and *m* indicate spectral parts for which the integration ranges were determined, see manuscript's main text and Fig. 2), at each temperature value:

$$\Delta = \frac{I_n}{I_m}$$

The relative thermal sensitivity (S_r) of the RENPs was calculated as:

$$S_r = \frac{1}{\Delta}\frac{\partial \Delta}{\partial T}$$

Selected $LiLuF_4$: 2.5 mol% Nd^{3+}/$LiLuF_4$ RENPs were further characterized in terms of their temperature uncertainty (δT), repeatability (R), and temporal uncertainty (δt).

Temperature uncertainty, δT, was measured by performing 200 consecutive spectral measurements at a fixed temperature (T_s = 28 ºC). δT was then estimated as standard deviation from the measured valued.

Repeatability parameter, R, was calculated as:

$$R = 1 - \frac{max(|\Delta_c - \Delta_i|)}{\Delta_c}$$

Where Δ_c is the mean PL intensity ratio value extracted from the calibration curve and Δ_i is that of each measurement for the repetitive heating-cooling cycles.

Temporal uncertainty, δt, of the RENPs was determined from the thermal relaxation curves obtained from *ex vivo* heating-cooling experiments, following the definition:

$$\delta t = \delta T \Big/ \left|\frac{\partial T}{\partial t}\right|_{max}$$

Where $|dT/dt|_{max}$ is the maximum temperature change per unit of time.

Ex vivo experiments

NIR images were acquired with an InGaAs NIR imaging camera (XEVA-1781, Xenics, Belgium). NIR emission light was collected after passing through an 830, 980 or 1150 nm LP filter.

For PL transmission experiments (Scheme S1), an aqueous dispersion of RENPs (5 mg/mL) was excited with 793 nm light of 49 W/cm^2 power density, and the PL trace was imaged maintaining a 90° optical geometry between the excitation beam and the NIR camera objective. Pork fat tissue of various thicknesses (1 to 10 mm) was placed between the PL trace and NIR camera.

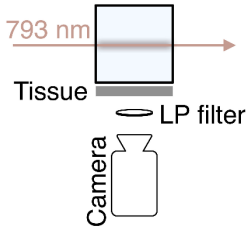

Scheme 1. Set-up of PL detection through pork fat tissue.

NIR imaging of glass capillary filled with an aqueous dispersion of RENPs (5 mg/mL) was done in a similar manner described above, this time also exciting RENPs through the tissue. A glass capillary (0.2 mm thick, 2 mm wide, with 0.15 mm wall thickness; Electron Microscopy Sciences, USA) containing RENPs was placed behind pork fat tissue of various thicknesses (1 to 5 mm). 793 nm laser (0.5 W/cm^2 impinging on the surface of the tissue) was used to excite the sample, and PL was collected with NIR camera placed in front of the tissue (Scheme 2).

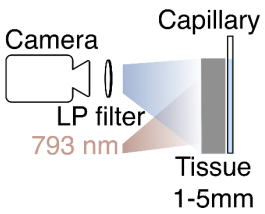

Scheme 2. Capillary imaging set-up through pork fat tissue.

Heating-cooling dynamics of an aqueous dispersion of RENPs (5 mg/mL) were measured irradiating the sample with 793 (~ 49 W/cm^2) and 980 nm (~ 37 W/cm^2) light, and placing the pork fat tissue of various thicknesses (1 to 5 mm) in front of the emission collecting lens (Scheme 3). The 793 nm laser was continuously exciting the RENPs for the duration of a single 12 min experiment. The PL (emission around 1050 nm: $^4F_{3/2} \rightarrow {}^4I_{11/2}$ transition and its thermometric parameter Δ_2) was used to spectrally determine the temperature in the vicinity of RENPs. Temperature increase was induced by simultaneously turning ON the 980 nm laser at the 2 min mark thereby heating the solution for 5 min after which it was switched OFF. Each measurement was repeated 5 times. A type K thermocouple (Mini-Hypodermic Probe, needle diameter of 0.2 mm; Omega, USA) connected to a type K handheld thermometer of 0.1 ºC (HH306A; Omega, USA) was used for contact measurement of temperature change inside the cuvette.

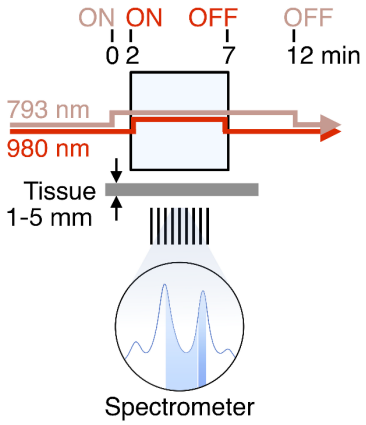

Scheme 3. Set-up of heating-cooling measurements through pork fat tissue.

TEM images of $LiLuF_4$: *x* mol% Nd^{3+}/$LiLuF_4$ ($LiYF_4$) RENPs

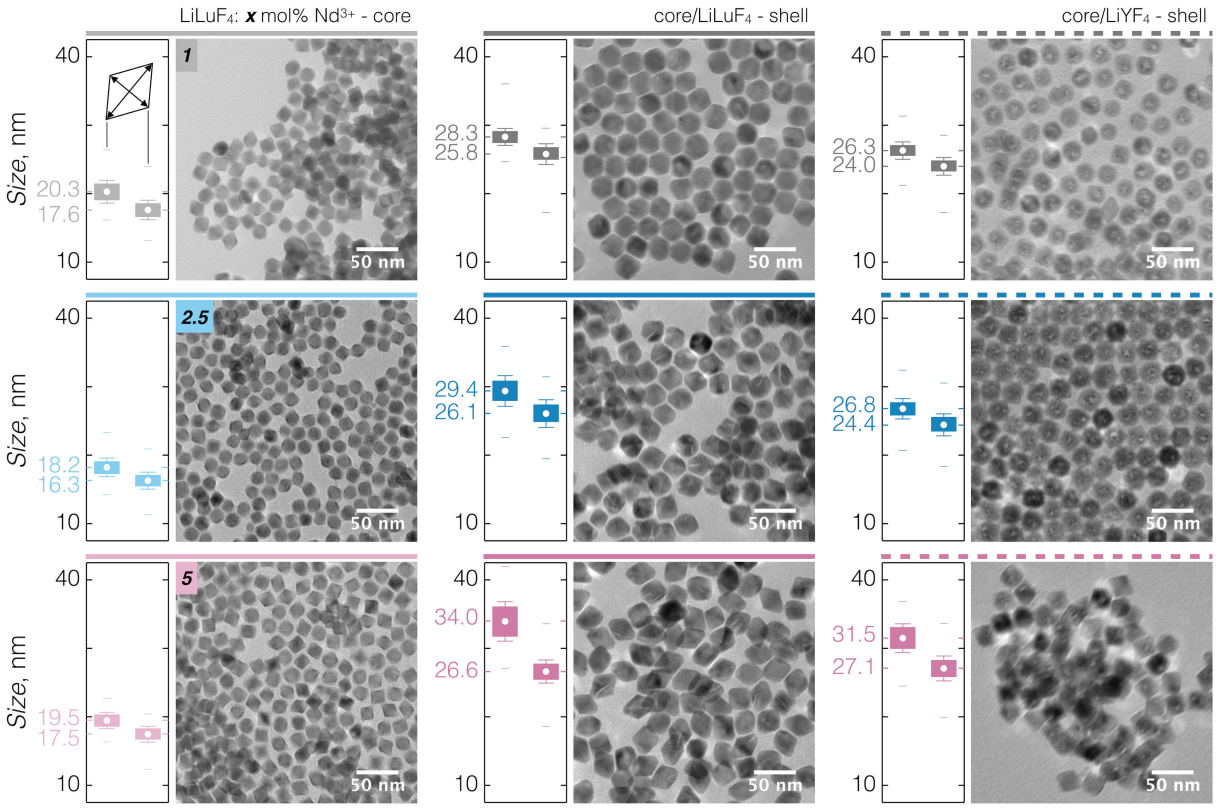

Figure S1. TEM images of $LiLuF_4$: ***x*** mol% Nd^{3+} - core and core/$LiLuF_4$ ($LiYF_4$) - shell RENPs and their respective size distribution measured along major and minor axes of an elliptical fit. Inset shows directions along which the size of the RENPs was measured. Box plots indicate: mean value (dot), 25th and 75th percentiles (box outline), SD (whiskers), and outliers (dashes).

XRD patterns of $LiLuF_4$: *x* mol% Nd^{3+}/$LiLuF_4$ ($LiYF_4$) RENPs

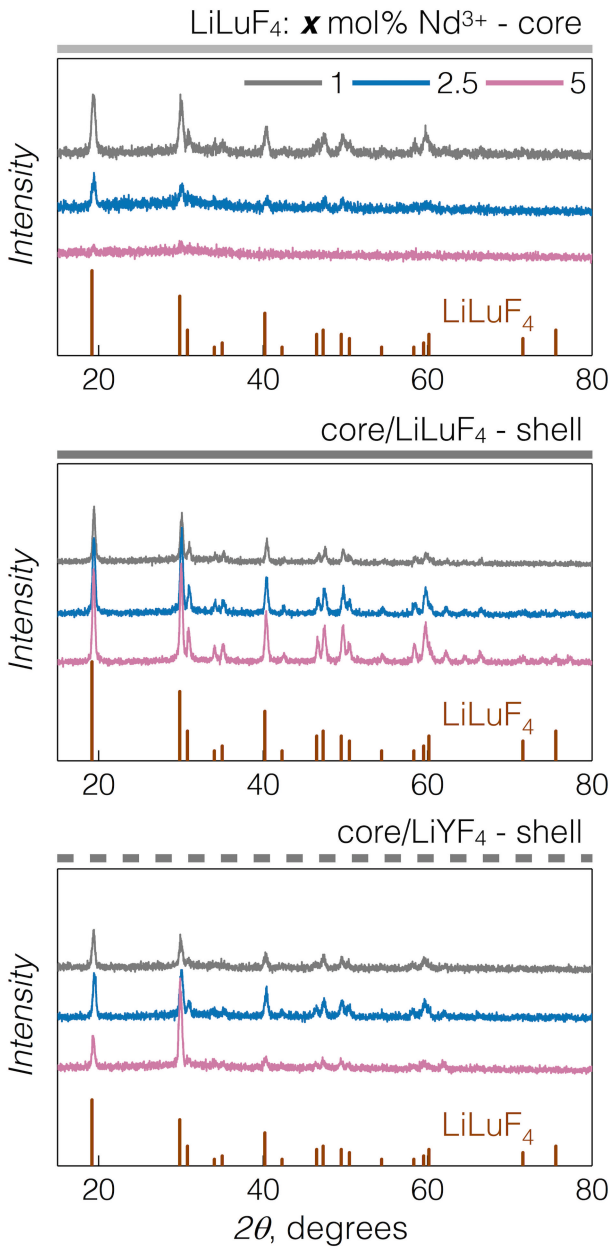

Figure S2. XRD patterns of $LiLuF_4$: ***x*** mol% Nd^{3+} - core and core/$LiLuF_4$ ($LiYF_4$) - shell RENPs, diffraction peaks of pure tetragonal $LiLuF_4$ crystal are also shown.

Attempted $LiGdF_4$ shelling

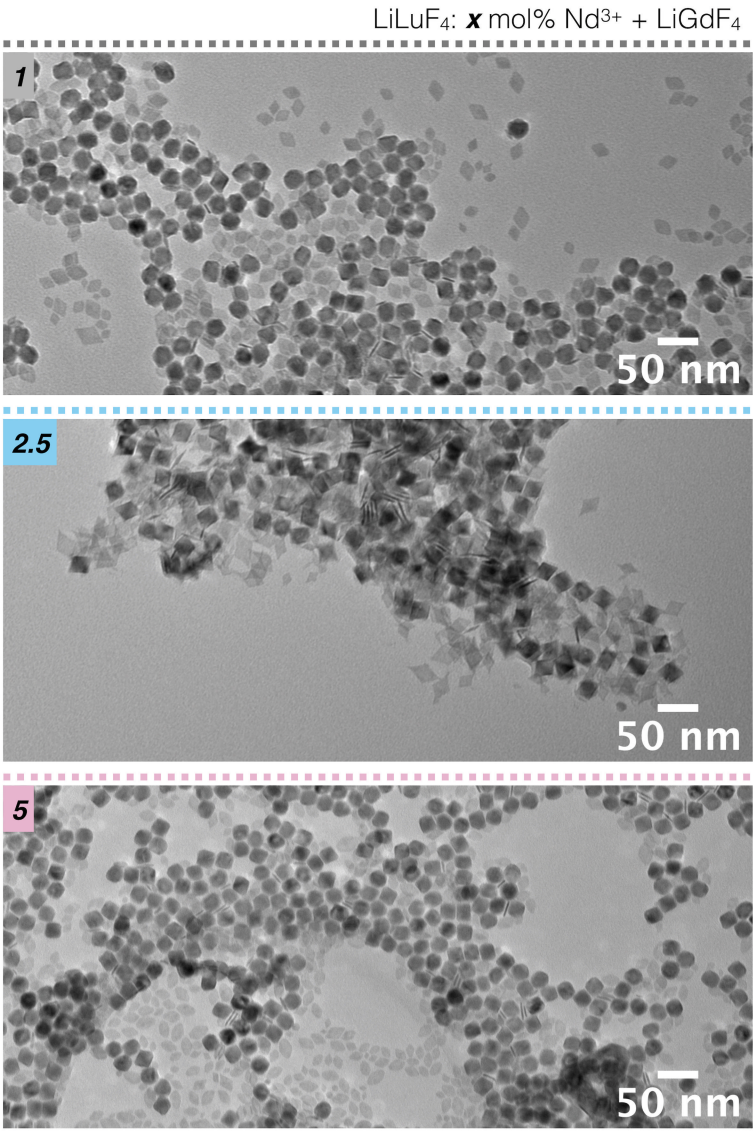

Figure S3. TEM images of $LiLuF_4$: ***x*** mol% Nd^{3+} RENPs after attempted shelling with Li^+ and Gd^{3+} trifluoroacetate precursors. Although slight size increase and change in the morphology of core RENPs can be noticed, two distinct populations of nanoparticles of different size and morphology are observed. The low contrast nanoparticles are tentatively ascribed to $LiGdF_4$.

PL spectra of $LiLuF_4$: *x* mol% Nd^{3+}/$LiLuF_4$ ($LiYF_4$) RENPs

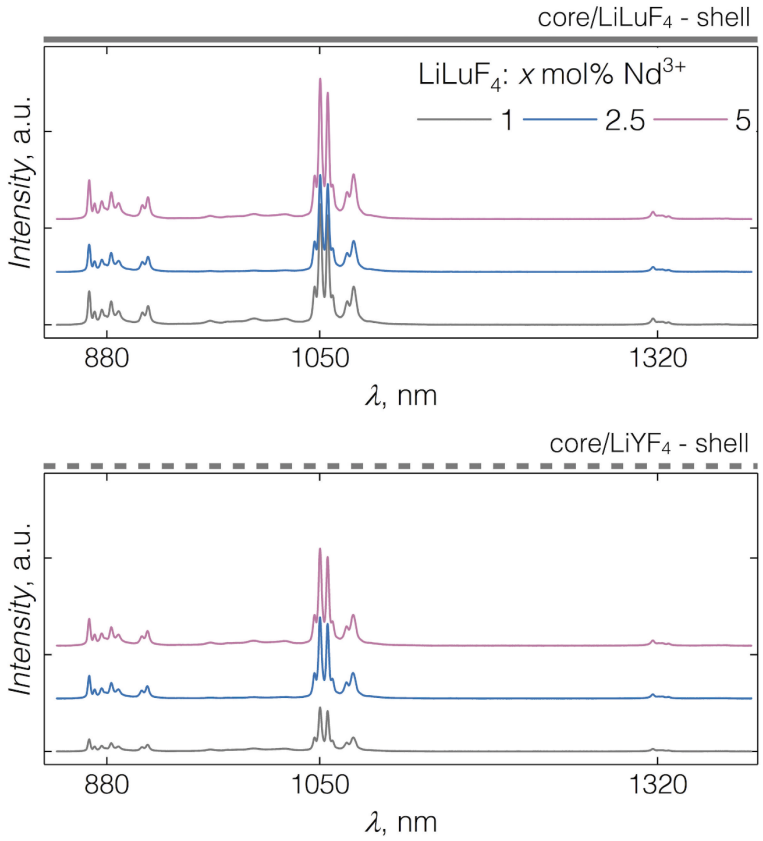

Figure S4. NIR PL spectra of aqueous dispersions of core/$LiLuF_4$ and core/$LiYF_4$ RENPs excited by 793 nm laser (power density 49 W/cm^2).

Comparison of S_r

Table S1. Comparison of single-band Nd^{3+} PL nanothermometers.

Nanoparticles	λ_{ex} (nm)	~λ_{em} *used for LIR* (nm)	*Max* S_r (* 10^{-2} °C^{-1})	*Reference*
$^4F_{3/2} \rightarrow {}^4I_{9/2}$				
$NaYF_4:Nd^{3+}$	830	867/870	0.097	D. Wawrzynczyk et al. (*Nanoscale* 2012)[4]
$LaF_3:Nd^{3+}$	808	885/863	0.100	U. Rocha et al. (*ACS Nano* 2013)[5]
$NaNdF_4/NaYF_4$/ $NaYF_4:Nd^{3+}$	808	R_2, $R_1 \rightarrow Z_1$ in 850-900 range	0.110	Ł. Marciniak et al. (*Nanoscale* 2017)[6]
Nd:YAG	808	938/946	0.150	A. Benayas et al. (*Adv. Opt. Mater.* 2015)[7]
$YVO_4:Nd^{3+}$	808	879/887	0.190	I. E. Kolesnikov et al. (*Sens. Actuator B 2016*)[8]
$LiNdP_4O_{12}$	808	R_2, $R_1 \rightarrow Z_1$ in 850-900 range	0.250	Ł. Marciniak et al. (*J. Lumin.* 2016)[9]
$LaF_3:Nd^{3+}$	808	865/885	0.260	E. Carrasco et al. (*Adv. Funct. Mater.* 2015)[10]
$LiLaP_4O_{12}:Nd^{3+}$ $KLaP_4O_{12}:Nd^{3+}$ $NaLaP_4O_{12}:Nd^{3+}$ $RbLaP_4O_{12}:Nd^{3+}$	830	R_2, $R_1 \rightarrow Z_1$ in 850-900 range	0.312 0.098 0.104 0.108	Ł. Marciniak et al. (*J. Mater. Chem. C* 2016)[11]
$LaF_3:Nd^{3+}$	808	861/863 885/865	0.400 0.200	U. Rocha et al. (*J. Lumin.* 2016)[12]
$LiLuF_4:Nd^{3+}$/ $LiLuF_4$	808	862/866	0.620	P. Huang et al. (*Adv. Sci.* 2019)[13]
$LiLuF_4:Nd^{3+}$/ $LiLuF_4$	793	887/883 887/913	0.580 0.580	This work
$^4F_{3/2} \rightarrow {}^4I_{11/2}$				
$YVO_4:Nd^{3+}$	808	1062/1072	0.150	I. E. Kolesnikov et al. (*Sens. Actuator B 2016*)[8]
$Y_2O_3:Nd^3$	808	1055/1076	0.150	I. E. Kolesnikov et al. (*Nanotechnology. 2019*)[14]
$Nd:KGd(WO_4)_2$	808	1075.8/1067.6	0.165	OI. A. Savchuk et al. (*J. Mat. Chem. C* 2016)[15]
$SrF_2:Nd^{3+},Y^{3+}$	808	1053/1062	0.180	M. Quintanilla et al. (*Chem. Mater.* 2018)[16]
$LiYF_4:Tm^{3+},Yb^{3+}$/ $LiYF_4/LiYF_4:Nd^{3+}$	806	1046.4/1056.7	0.223	A. Skripka et al. (*Adv. Funct. Mater.* 2019)[17]
$YVO_4:Nd^{3+}$	808	1063/1070	0.250	I. E. Kolesnikov et al. (*Sens. Actuator B 2017*)[18]
$YVO_4:Nd^{3+}$	808	1064.8/1066.3 (integral) 1064.8/1063.7 (integral) 1064.8/1066.3 (point) 1064.8/1063.7 (point)	0.350 0.320 0.480 0.470	I. E. Kolesnikov et al. (*J. Lumin. 2017*)[19]
$YVO_4:Nd^{3+}/SiO_2$	808	1064.7/1066.3	0.400	I. E. Kolesnikov et al. (*J. Alloys Compd. 2018*)[20]
$Y_2O_3:Nd^{3+}$	808	1053/1075 1057/1080	0.430 0.370	I. E. Kolesnikov et al. (*J. Lumin. 2018*)[21]
$LiLuF_4:Nd^{3+}$/ $LiLuF_4$	793	1047/1056 1053/1056	0.480 0.480	This work
$^4F_{3/2} \rightarrow {}^4I_{13/2}$				
$(Gd_{0.980}Nd_{0.020})_2O_3$	808	R_2, $R_1 \rightarrow Z_j$ in 1250-1500 range	0.230	S. Balabhadra et al. (*J. Lumin.* 2016)[22]
$LiLuF_4:Nd^{3+}$/ $LiLuF_4$	793	1322/1328	0.490	This work

S_r of pure PL ratio nanothermometer

PL ratio nanothermometry, based on two emission bands (I_n and I_m) stemming from thermally coupled electronic levels, is described by the Boltzmann distribution:

$$\Delta = \frac{I_n}{I_m} = Bexp\left(-\frac{\Delta E}{k_B T}\right)$$

where ΔE is the energy gap separating the thermally coupled electronic levels, k_B is Boltzmann's constant, T is temperature and B is:

$$B = \frac{c_n(\nu)A_n g_n h\nu_n}{c_m(\nu)A_m g_m h\nu_m}$$

here, A_i (i = n, m) and g_i are the spontaneous emission rates and degeneracies of the emitting thermally coupled electronic states, $c_i(\nu)$ is the spectral response of the experimental system at the emission frequency ν_i, and h is Planck's constant.

Taking the general expression of relative sensitivity for a thermometer, we then can calculate the S_r value attainable for a given PL ratio governed nanothermometric system as:

$$S_R = \frac{1}{\Delta}\left|\frac{\Delta}{T}\right| = \frac{\Delta E}{k_B T^2}$$

In the case of the studied Nd^{3+} doped RENPs, the thermally coupled energy levels of Nd^{3+} are $^4F_{3/2}$ (R_1) and $^4F_{3/2}$ (R_2) with ΔE ~ 55 cm^{-1} (Figure S5). This would result in S_r ~ 0.09 %·ºC^{-1} at 20 ºC for any purely PL ratio based thermometric parameter defined for our RENPs.

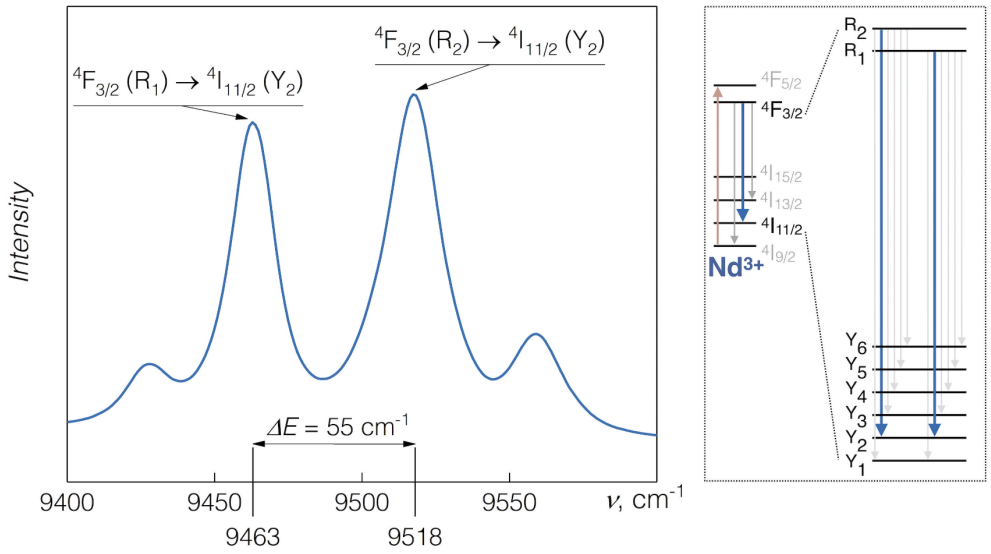

Figure S5. PL spectra of RENPs under 793 nm excitation, showing PL band around 1050 nm ($^4F_{3/2} \rightarrow {}^4I_{11/2}$ radiative transition; see scheme on the right) with its Stark structure. From the peak positions of the most intense Stark bands, an energy gap $\Delta E \sim 55$ cm^{-1} between the R_2 and R_1 sub-levels of $^4F_{3/2}$ electronic state can be calculated.

Quantum efficiency of NIR detector

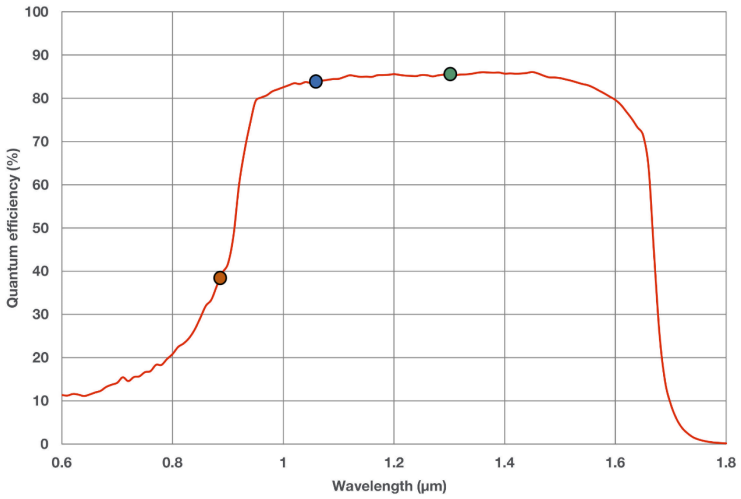

Figure S6. Quantum efficiency of the InGaAs NIR detector used in our NIR spectrum acquisition setup. Approximate positions of Nd^{3+} radiative transitions are labeled with dots: red - $^4F_{3/2} \rightarrow {}^4I_{9/2}$ ~ 880 nm, blue - $^4F_{3/2} \rightarrow {}^4I_{11/2}$ ~ 1050 nm, and green - $^4F_{3/2} \rightarrow {}^4I_{13/2}$ ~ 1320 nm. Data was adapted from the specification provided by the manufacturer (https://andor.oxinst.com/assets/uploads/products/andor/documents/Andor-iDus-InGaAs-1.7-Specifications.pdf)

Repeatability of RENPs as NIR nanothermometers

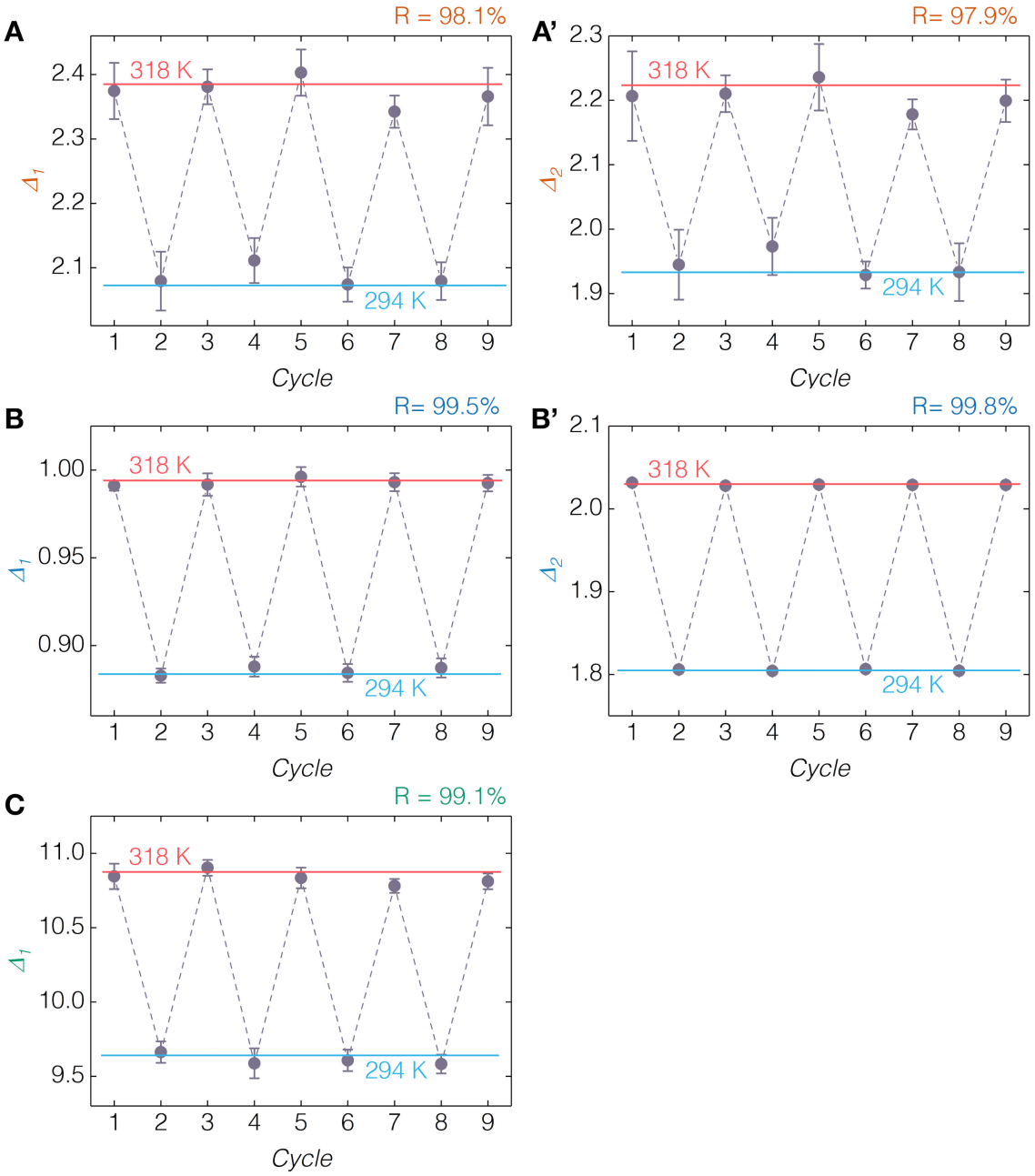

Figure S7. Repeatability parameter, *R*, for the different thermometric parameters of RENPs, evaluated from measuring temperature following multiple heating-cooling cycles. A – Δ_1 and A' – Δ_2 of the $^4F_{3/2} \rightarrow {}^4I_{9/2}$ emission; B – Δ_1 and B' – Δ_2 of the $^4F_{3/2} \rightarrow {}^4I_{11/2}$ emission; C – Δ_1 of the $^4F_{3/2} \rightarrow {}^4I_{13/2}$ emission.

Invariability of 1050 nm emission

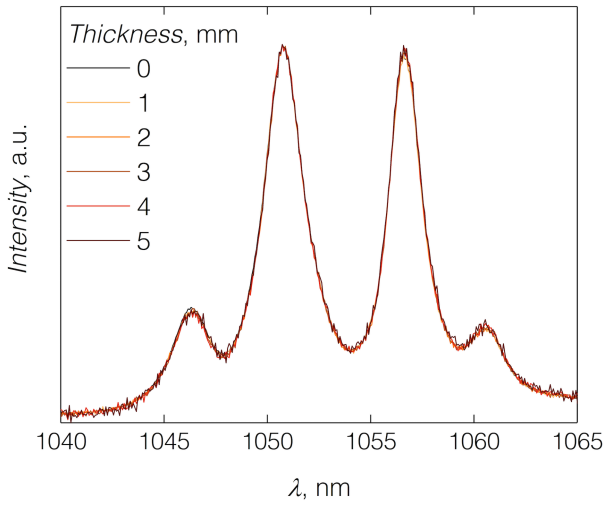

Figure S8. PL spectra (normalized to maximum of intensity) of RENPs under 793 nm excitation, collected before and after propagating through pork fat tissue of different thickness (from 1 to 5 mm).

S_r of $LiLuF_4$: *x* mol% Nd^{3+}/$LiLuF_4$ ($LiYF_4$) RENPs

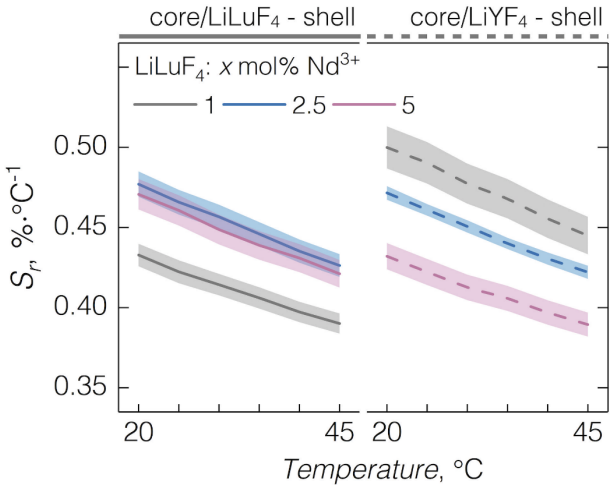

Figure S9. S_r values of thermometric parameter Δ_2 of the $^4F_{3/2} \rightarrow {}^4I_{11/2}$ emission for different $LiLuF_4$: ***x*** mol% Nd^{3+}/$LiLuF_4$ ($LiYF_4$) RENPs.

PL transmission through pork fat tissue

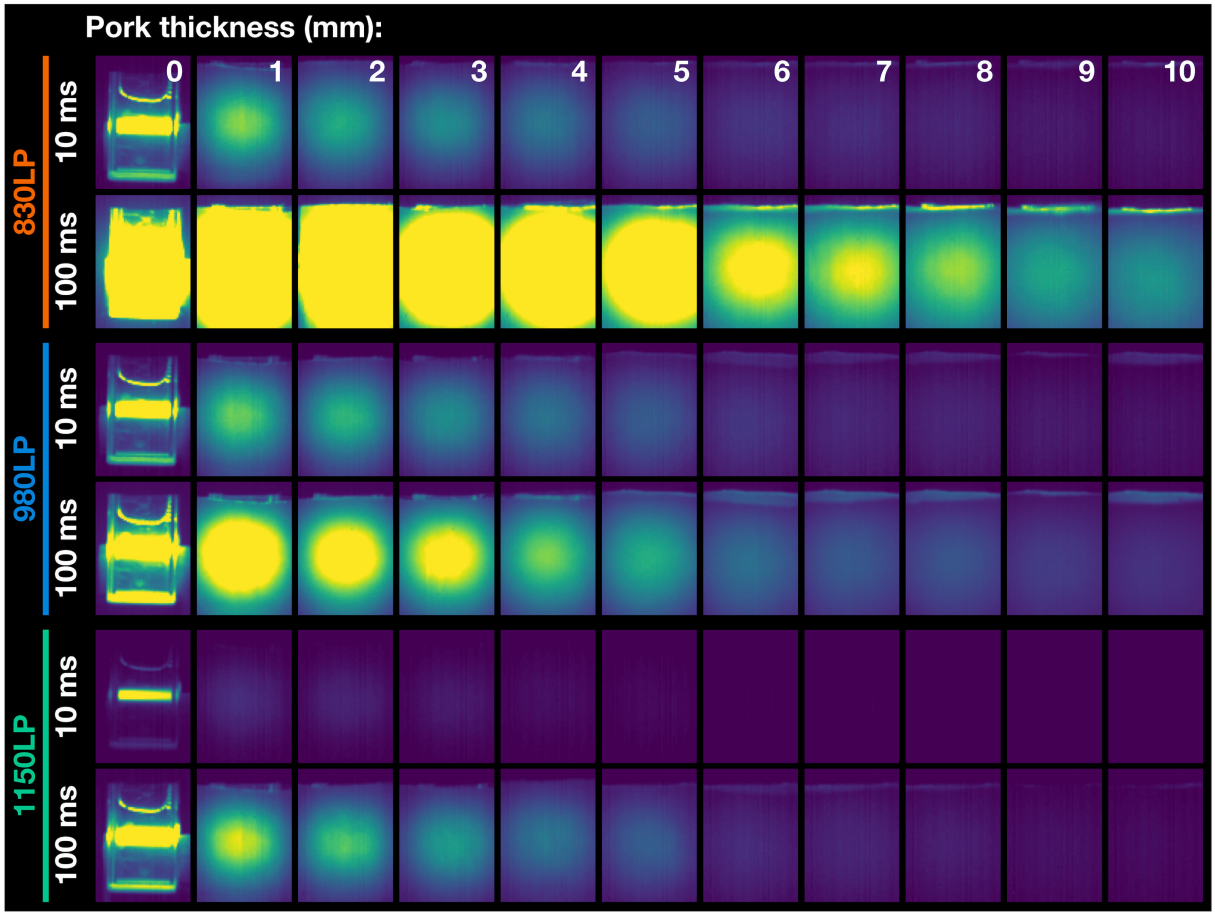

Figure S10. NIR images of the PL emission of RENPs excited with a 793 nm laser and observed through varying thickness of pork fat tissue. Different LP filters were applied to first exclude contributions of PL around 880 (980LP) and then 1050 nm (1150LP). Images were acquired with 10 and 100 ms of exposure time.

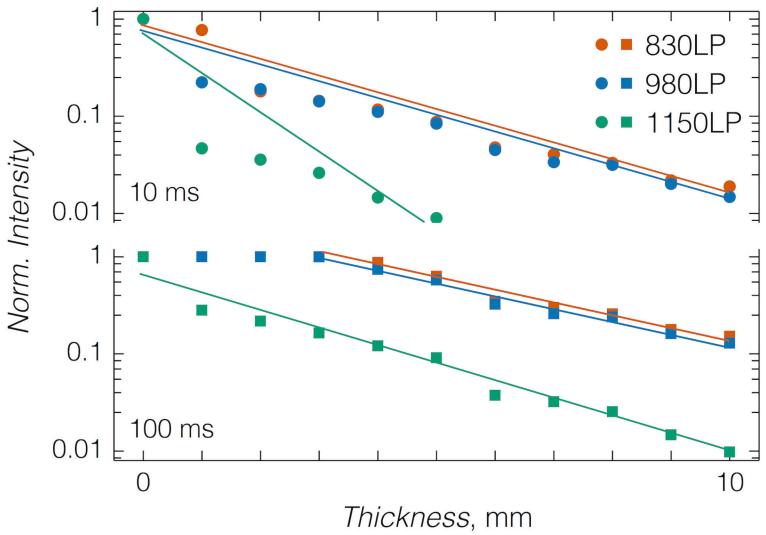

Figure S11. Intensity change around the center of the PL trace as the emitted light was passing through increasing thickness of pork fat tissue. Intensities are normalized to the “no tissue” initial signal. Lines are guides for the eye.

Heating-cooling characterization

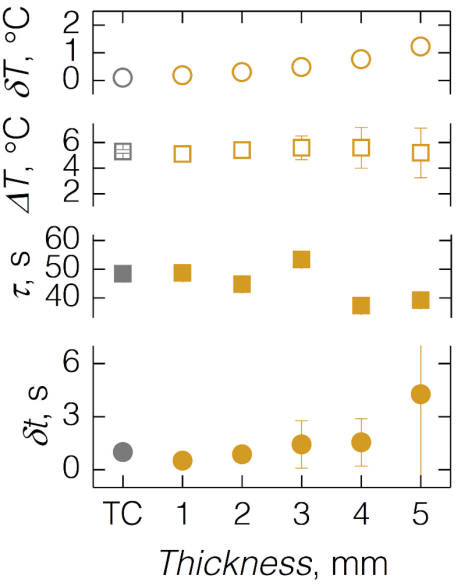

Figure S12. Representation of thermal (δT) and temporal (δt) uncertainty changes with increasing thickness of pork fat tissue in the heating-cooling *ex vivo* experiment. ΔT is temperature increase induced by the 980 nm laser and τ is the relaxation time obtained from the single-exponential fit of the cooling curves (Fig. 6 of the main text). Grey points indicate the respective value obtained based on the contact TC measurement.

References

[1] T. Cheng, R. Marin, A. Skripka, F. Vetrone, *J. Am. Chem. Soc.* **2018**, 140, 12890.

[2] N. Bogdan, F. Vetrone, G. A. Ozin, J. A. Capobianco, *Nano Lett.* **2011**, 11, 835.

[3] C. D. S. Brites, A. Millán, L. D. Carlos, in *Handbook on the Physics and Chemistry of Rare Earths*, Vol. 49 (Eds: B. Jean-Claude, P. Vitalij K), Elsevier **2016**, p. 339.

[4] D. Wawrzynczyk, A. Bednarkiewicz, M. Nyk, W. Strek, M. Samoc, *Nanoscale* **2012**, 4, 6959.

[5] U. Rocha, C. Jacinto da Silva, W. Ferreira Silva, I. Guedes, A. Benayas, L. Martinez Maestro, M. Acosta Elias, E. Bovero, F. C. van Veggel, J. A. Garcia Sole, D. Jaque, *ACS Nano* **2013**, 7, 1188.

[6] L. Marciniak, A. Pilch, S. Arabasz, D. Jin, A. Bednarkiewicz, *Nanoscale* **2017**, 9, 8288.

[7] A. Benayas, B. del Rosal, A. Pérez-Delgado, K. Santacruz-Gómez, D. Jaque, G. A. Hirata, F. Vetrone, *Adv. Opt. Mater.* **2015**, 3, 687.

[8] I. E. Kolesnikov, E. V. Golyeva, M. A. Kurochkin, E. Lähderanta, M. D. Mikhailov, *Sens. Actuators B-Chem.* **2016**, 235, 287.

[9] L. Marciniak, K. Prorok, A. Bednarkiewicz, A. Kowalczyk, D. Hreniak, W. Strek, *J. Lumin.* **2016**, 176, 144.

[10] E. Carrasco, B. del Rosal, F. Sanz-Rodríguez, Á. J. de la Fuente, P. H. Gonzalez, U. Rocha, K. U. Kumar, C. Jacinto, J. G. Solé, D. Jaque, *Adv. Funct. Mater.* **2015**, 25, 615.

[11] Ł. Marciniak, A. Bednarkiewicz, D. Hreniak, W. Strek, *J. Mater. Chem. C* **2016**, 4, 11284.

[12] U. Rocha, C. Jacinto, K. U. Kumar, F. J. López, D. Bravo, J. G. Solé, D. Jaque, *J. Lumin.* **2016**, 175, 149.

[13] P. Huang, W. Zheng, D. Tu, X. Shang, M. Zhang, R. Li, J. Xu, Y. Liu, X. Chen, *Adv. Sci.* **2019**, 6, 1802282.

[14] I. E. Kolesnikov, A. A. Kalinichev, M. A. Kurochkin, D. V. Mamonova, E. Yu. Kolesnikov, E. Lähderanta and M. D. Mikhailov, *Nanotechnology*, 2019, **30**, 1345501.

[15] O. Savchuk, J. J. Carvajal, L. G. De la Cruz, P. Haro-Gonzalez, M. Aguilo, F. Diaz, *J. Mater. Chem. C* **2016**, 4, 7397.

[16] M. Quintanilla, Y. Zhang, L. M. Liz-Marzán, *Chem. Mater.* **2018**, 30, 2819.

[17] A. Skripka, V. Karabanovas, G. Jarockyte, R. Marin, V. Tam, M. Cerruti, R. Rotomskis, F. Vetrone, *Adv. Funct. Mater.* **2019**, 29, 1807105.

[18] I. E. Kolesnikov, E. V. Golyeva, A. A. Kalinichev, M. A. Kurochkin, E. Lähderanta, M. D. Mikhailov, *S. Actuators B-Chem.* **2017**, 243, 338.

[19] I. E. Kolesnikov, A. A. Kalinichev, M. A. Kurochkin, D. V. Mamonova, E. Y. Kolesnikov, A. V. Kurochkin, E. Lähderanta, M. D. Mikhailov, *J. Lumin.* **2017**, 192, 40.

[20] I. E. Kolesnikov, M. A. Kurochkin, A. A. Kalinichev, D. V. Mamonova, E. Y. Kolesnikov, A. V. Kurochkin, E. Lähderanta, M. D. Mikhailov, *J. Alloy. Compd.* **2018**, 734, 136.

[21] I. E. Kolesnikov, A. A. Kalinichev, M. A. Kurochkin, D. V. Mamonova, E. Y. Kolesnikov, A. V. Kurochkin, E. Lähderanta, M. D. Mikhailov, *J. Lumin.* **2018**, 204, 506.

[22] S. Balabhadra, M. L. Debasu, C. D. S. Brites, J. Rocha, L. D. Carlos, *J. Lumin.* **2016**, 180, 25.